Mon. Not. R. Astron. Soc. **312**, 724–732 (2000)

Constraints on structure formation models from the Sunyaev–Zel'dovich effect

Subhabrata Majumdar[1,2]★ and Ravi Subrahmanyan[3,4]★

[1]*Joint Astrophysics Programme, Department of Physics, Indian Institute of Science, Bangalore 560 012, India*
[2]*Indian Institute of Astrophysics, Koramangala, Bangalore 560 034, India*
[3]*Australia Telescope National Facility, CSIRO, Locked bag 194, Narrabri, NSW 2390, Australia*
[4]*Raman Research Institute, Sadashivanagar, Bangalore 560 080, India*

Accepted 1999 October 11. Received 1999 September 9; in original form 1999 June 28

ABSTRACT

In the context of cold dark matter (CDM) cosmological models, we have simulated images of the brightness temperature fluctuations in the cosmic microwave background (CMB) sky owing to the Sunyaev–Zel'dovich (S–Z) effect in a cosmological distribution of clusters. We compare the image statistics with recent ATCA limits on arcmin-scale CMB anisotropy. The S–Z effect produces a generically non-Gaussian field and we compute the variance in the simulated temperature-anisotropy images, after convolution with the ATCA beam pattern, for different cosmological models. All the models are normalized to the 4-yr *COBE* data. We find an increase in the simulated-sky temperature variance with increase in the cosmological density parameter Ω_0. A comparison with the upper limits on the sky variance set by the ATCA appears to rule out our closed-universe model: low-Ω_0 open-universe models are preferred. The result is independent of any present day observations of σ_8.

Key words: galaxies: clusters: general – cosmic microwave background – cosmology: observations – cosmology: theory.

1 INTRODUCTION

A key problem in modern cosmology is the determination of the geometry of the universe. Classical methods of deriving the cosmological parameters involve measurements of the redshift dependence of apparent luminosities of 'standard candles', or the angular sizes of 'standard rulers', or the number densities of non-evolving objects. These methods are expected to probe the background geometry independent of any structure formation. Many of these classical approaches have been limited by the difficulties in identifying objects, distributed over cosmic time-scales, that are untouched by astrophysical evolution; however, it may be noted that progress has recently been reported using supernovae Type 1a as standard candles (Perlmutter et al. 1998).

The formation of structure is dependent on the background cosmology. Attempts have been made to exploit this coupling by examining the parameter space allowed for the cosmological constants by favoured models of structure formation. Motivated by the discovery of anisotropy in the cosmic microwave background (CMB), progress in the understanding of physical mechanisms responsible for the anisotropy spectrum and the influence of the background cosmology in the generation of these anisotropies have led to attempts at deriving constraints on the cosmological parameters from the shape of the CMB anisotropy spectrum (Bond et al. 1994). Anisotropies in the CMB are usually described by its power spectrum: $C_l = \langle |C_{lm}|^2 \rangle$ represents the anisotropy power at multipole order l, where C_{lm} are the coefficients of the spherical harmonic decomposition of the fractional temperature fluctuations. The density fluctuations that are hypothesized to have been generated in the very early universe are believed to grow via gravitational instabilities and give rise to the large scale structures we see in the present day universe. The CMB temperature fluctuations seen today on large angular scales exceeding about a degree are believed to be a direct consequence of matter inhomogeneities on scales exceeding $\approx$100 Mpc at the recombination epoch. The gravitational and astrophysical evolution, in the post-recombination universe, which led to the formation of galaxies and their clustering, may have altered these primary radiation anisotropies and may have given rise to the dominant CMB fluctuations on small angular scales. Since the generation of the CMB anisotropies and their appearance on the sky is intimately linked with the background cosmology, the study of CMB anisotropies on different scales give constraints on theories of structure formation and also on the parameters of cosmological models.

Anisotropies in the CMB are divided broadly into two classes: primary and secondary anisotropies. The primary anisotropies are those generated at the last scattering surface. The angular power spectrum of these anisotropies, as seen by observers at the present

★ E-mail: sum@physics.iisc.ernet.in (SM); Ravi.Subrahmanyan@atnf.csiro.au (RS)

epoch, depends on the parameters of the background cosmology – the Hubble constant H_o, the mean matter density Ω_o and the constituents of the matter (i.e. the amount of baryonic matter, cold dark matter, hot dark matter etc.) and any cosmological constant Λ – and on the magnitude and spectrum of primordial perturbations in the matter. Several authors have derived the marginal and joint dependencies of the cosmological parameters on characteristic features in the CMB anisotropy spectrum. For example, at large and intermediate angular scales ($l \leqslant 500$), for $\Omega_0 < 1$, the Doppler peaks in the CMB anisotropy spectrum are shifted towards larger l values (see, for example, Kamionkowski & Spergel 1994 or Lineweaver & Barbosa 1998). The ionization history modifies the radiation spectrum and serves to attenuate power at high-order multipoles. Primary anisotropies at small angular scales ($l \geqslant 500$) are expected to be relatively damped in most models of structure formation due to the thickness of the last scattering surface and the diffusion damping of sub-horizon scale baryon fluctuations in the pre-recombination era; anisotropies at even larger l may be critically dependent on the reionization history.

The secondary anisotropies arise due to interactions between the growing matter perturbations and the CMB photons as they travel from the last-scattering-surface to the present time. Arcmin-scale anisotropies may be generated due to second-order mode coupling between density perturbations and bulk velocities (Hu, Scott & Silk 1994; Persi et al. 1995). Separately, decrements in the CMB sky may be generated owing to the inverse-Compton scattering of background photons as they pass through concentrations of hot gas associated with clusters of galaxies along the line of sight; this phenomenon is referred to as the Sunyaev Zel'dovich (S–Z) effect. A dominant contribution to the anisotropy power at large l may come from quasar-ionised hot gas bubbles (Aghanim et al. 1996).

Among the various effects that may give rise to CMB anisotropy on small angular scales, we focus on the S–Z effect in this work. In Section 2, we discuss some details of the S–Z effect and in Section 3, we discuss some of the motivations for attempting to constrain cosmological models using the S–Z effect. In Section 4, we present the formalism we have adopted for deriving the expectations for CMB anisotropy on small angular scales for specific models of structure formation. The results of simulations of sky temperature anisotropy are compared with ATCA limits on arcmin-scale anisotropy to derive constraints on the cosmological density parameter Ω_o.

2 THE SUNYAEV–ZEL'DOVICH EFFECT

The hot intracluster gas inverse-Compton scatters the CMB photons propagating through the cluster medium, and the energy transfer in this interaction between the hot electrons and CMB photons results in a distortion to the CMB spectrum (Sunyaev & Zel'dovich 1972). The integral of the electron pressure along any line-of-sight through the cluster determines the magnitude of the distortion in that direction, this is quantified in terms of the Compton y-parameter:

$$y = \int \mathrm{d}l \frac{k(T_\mathrm{e} - T_\gamma)}{m_\mathrm{e}c^2} n_\mathrm{e}\sigma_\mathrm{T}, \tag{1}$$

where k is the Boltzmann's constant, T_e and T_γ are, respectively, the kinetic temperature of the electron and the thermodynamic temperature of the incident black-body radiation, m_e is the electron rest mass, c is the velocity of light, n_e is the electron number density and σ_T is the Thomson scattering cross-section.

The S–Z effect manifests itself as a change in sky brightness

$$\delta i_\nu = y j_\nu(x), \tag{2}$$

towards the cluster with respect to the mean CMB intensity. x is a dimensionless frequency parameter defined to be

$$x = \frac{h\nu}{kT_\mathrm{o}}, \tag{3}$$

where h is Planck's constant, ν is the observing frequency and T_o is the CMB temperature at the present epoch: $T_\mathrm{o} = 2.73\,\mathrm{K}$. The frequency dependence of the change in sky brightness, owing to the S–Z effect, is given by

$$j_\nu(x) = \frac{2(kT_\mathrm{o})^3}{(hc)^2} \frac{x^4 e^x}{(e^x - 1)^2} \left[\frac{x}{\tanh(x/2)} - 4\right]. \tag{4}$$

The spectral function has a unique shape owing to the fact that although there is a net transfer of energy from the hot electron gas to the radiation, inverse-Compton scattering conserves the total number of photons and the mean photon energy is increased. The result is that there is a net diffusion of photons upwards in energy. Assuming the cluster electron temperature to be about 10 keV, the net distortion observed is expected to be zero at about 222 GHz (1.35 mm wavelength), the distortion is expected to result in a decrement in the brightness temperature towards the cluster at lower frequencies and the cluster will be seen as a positive source at higher frequencies.

At wavelengths longward of 1.35 mm, a cluster appears as a negative source on the sky with respect to the mean CMB background intensity: the flux density S_ν due to the integrated S–Z effect over the sky area of a cluster is

$$S_\nu(x) = \frac{j_\nu(x)}{D_\mathrm{a}^2(z)} \int \mathrm{d}V \frac{kT_\mathrm{e}}{m_\mathrm{e}c^2} n_\mathrm{e}\sigma_\mathrm{T}. \tag{5}$$

We have assumed that $T_\mathrm{e} \gg T_\gamma$. The integral extends over the cluster volume and $D_\mathrm{a}(z)$ is the angular-size distance to the cluster. It is clear from the equation above that the net S–Z effect due to a cluster is dependent only on the total mass of hot gas in the cluster and a density-weighted mean temperature. The S–Z flux density from a cluster diminishes as the square of its angular-size distance: because the angular-size distance of objects at cosmological distances, $z \gtrsim 1$, saturates to a limiting value or even decreases with increasing redshift, the S–Z flux from a cluster does not rapidly diminish with increasing cosmological distance. However, the distributions of cluster gas temperature and electron density may be functions of redshift; therefore, the expected S–Z flux density from a cluster may be redshift dependent.

It may be noted here that y is a dimensionless parameter and S_ν has units of $\mathrm{erg\,s^{-1}\,cm^2\,Hz^{-1}}$: this flux density is usually expressed in Jansky (Jy), defined as $1\,\mathrm{Jy} = 10^{-23}\,\mathrm{erg\,s^{-1}\,cm^2\,Hz^{-1}}$.

3 MOTIVATION FOR STUDYING THE S–Z EFFECT

The Sunyaev–Zel'dovich effect provides a rather nice and complementary approach to the traditional methods – which use X-ray temperature and X-ray luminosity evolution in clusters of galaxies – of studying the evolution of the mass function of collapsed objects (Bartlett 1997). The evolution in the abundance of clusters of galaxies is sensitive to the mean matter density Ω_o

and, consequently, is a useful constraint on cosmological models. The traditional method derives its faith from numerical simulations which show that there is a tight correlation between the virial mass and the emission-weighted X-ray temperature in clusters of galaxies (Evrard 1990, 1996). However, the traditional method has a major disadvantage: because of 'cosmological dimming', the surface brightness of distant X-ray sources falls off as $(1+z)^{-4}$, and for this reason, obtaining samples of clusters at cosmological distances can be observationally challenging. In the case of the S–Z effect in cosmological clusters, the decrement in brightness in lines of sight towards clusters of galaxies has the distinct advantage of being independent of the distance to the cluster. The S–Z flux density from a cluster will diminish with distance to the cluster as the square of the angular-size distance; this is in contrast to X-ray flux densities from clusters which diminish as the square of the luminosity distance to the cluster. Moreover, the integrated S–Z effect due to any cluster, i.e. the flux density decrement, is proportional to the total hot-gas mass times the particle-weighted temperature. Consequently, the detection of any cluster is independent of the gas' spatial distribution (assuming the cluster is unresolved). If the observations resolve clusters, particularly at lower redshifts, the observed sky temperature distribution will be sensitive to the temperature structure within the clusters; once again this may be contrasted with X-ray emission images of cluster gas distributions which are sensitive to the gas density distribution.

The S–Z effect may, therefore, be used as a tracer of clusters and other massive hot gaseous objects at cosmological distances. Because the redshift evolution of clusters is a sensitive probe of cosmology theory, the number counts of S–Z sources may be used to infer their cosmological abundances and thereby deduce parameters relating to the background cosmological model and the structure formation theory (see, for example, Blanchard & Bartlett 1998; Oukbir & Blanchard 1992, 1997). Motivated by this reasoning, several authors have, in recent years, made calculations of the expected S–Z source counts and their redshift distributions. These have been related to the cosmological parameters as well as the evolution in the intracluster medium (Bartlett & Silk 1994; Barbosa et al. 1996; Colafransesco et al. 1997).

As discussed in Section 2, clusters of galaxies may be 'visible', owing to the S–Z effect, as sources in the sky with a negative flux density at wavelengths longward of 1.35 mm and with a positive flux density at shorter wavelengths. This S–Z effect has been imaged to-date towards several clusters (see Birkinshaw 1999 for a recent review). We may consider distant cosmological clusters – observed at wavelengths longward of 1.35 mm – as a sky distribution of sources with negative flux density. Observational sensitivity in modern radio telescopes is reaching values close to that required for detecting the S–Z effect from cosmological clusters towards 'blank fields' where no obvious clusters are seen in either their optical or X-ray emission. There have been claims in the literature of the detection of radio decrements (thought to be due to the S–Z effect) in sensitive images made of 'blank' sky fields (Jones et al. 1996; Richards et al. 1996); however, sensitive observations of several other fields with arcmin resolution have failed to detect any decrements or CMB anisotropies (Subrahmanyan et al. 1998, 1999).

It may be noted here that because the S–Z effect has a generic non-Gaussian temperature distribution, it could be detected in a sky image by estimators sensitive to skewed variance. Many other secondary contributors to the temperature anisotropy have a Gaussian distribution in amplitudes; therefore, the negative-skewed-nature of the S–Z effect may be useful in distinguishing it from other sources, foregrounds and instrument noise.

4 SIMULATIONS

4.1 The cosmological distribution of clusters of galaxies

As discussed earlier, large-angle anisotropies in the microwave background radiation may be traced back to its generation from small-amplitude primordial density fluctuations in the early universe. The matter perturbations have since grown due to gravitational instabilities into the large scale structure we see at the present epoch. In addition, as the primeval CMB radiation propagated to us through growing matter inhomogeneities, astrophysical couplings give rise to secondary anisotropies on predominantly small angular scales. The power spectrum $P(k, z_{\rm eq})$ of the fractional density fluctuations, at the redshift $z = z_{\rm eq}$ when the energy densities in matter equalled that in radiation, may be related to the primordial power spectrum $P_p(k)$ by:

$$P(k, z_{\rm eq}) = T^2(k) \times P_p(k). \tag{6}$$

The matter transfer function $T(k)$ describes the processing of the initial density perturbations during the radiation dominated era (Padmanabhan 1993): the modifications to the shape of the perturbations would depend on the nature of the perturbations and the candidate dark matter. Thereafter, during the matter-dominated era, the dominant dark matter (DM) perturbations experience equal growth on all scales and $P(k, z)$ grows retaining its shape. The growth rate, described below by the growth function, varies with cosmic time and depends on the mean matter density $\Omega_{\rm o}$. Models of structure formation are usually characterized by specific $P(k, z_{\rm eq})$ shapes and normalizations.

For the purpose of our simulations, we wish to relate the number density of collapsed objects of different masses, at different cosmic epochs, to the initial density contrast on different scales, i.e. the initial matter spectrum $P(k, z_{\rm eq})$. It is assumed, in most theories of structure formation, that the initial small-amplitude density fluctuations are Gaussian random, i.e. the amplitudes are Gaussian distributed and that the fluctuations on different modes are uncorrelated (random phase fluctuations). Structure is believed to form from the growing perturbations hierarchically, with smaller-scale fluctuations collapsing first and larger scales later. The mass and redshift distribution of the number density $n(M, z)$ of collapsed objects may then be computed using the Press-Schechter formalism (Press & Schechter 1974; see Padmanabhan & Subramanian 1992 for a tutorial):

$$n(M, z)\,{\rm d}M = \sqrt{\frac{2}{\pi}}\,\frac{\langle\rho\rangle}{M}\,\nu_c \left|\frac{{\rm d}\ln\sigma(M, z)}{{\rm d}\ln M}\right| {\rm e}^{-\nu_{\rm c}^2/2}\,\frac{{\rm d}M}{M}, \tag{7}$$

where

$$\nu_{\rm c}(M, z) = \frac{\delta_{\rm c}}{\sigma(M, z)} = \frac{\delta_{\rm c} D_{\rm g}(0)}{\sigma_0(M) D_{\rm g}(z)}. \tag{8}$$

In these equations, $\langle\rho\rangle$ denotes the mean comoving matter density in the universe: $\langle\rho\rangle = 3\Omega_{\rm o}H_{\rm o}^2/(8\pi G)$, where $\Omega_{\rm o}$ is the density parameter, $H_{\rm o} = 100\,h\,{\rm km\,s^{-1}\,Mpc^{-1}}$ is the Hubble constant and G is the gravitational constant. $\sigma(M, z)$ denotes the rms fluctuations, at redshift z, in the fractional density contrast in the matter when smoothed to a mass scale $M = \frac{4}{3}\pi R^3\langle\rho\rangle$, where R

is the comoving radial length scale of the smoothing function. $\sigma_o(M)$ is the rms density contrast at the present epoch.

The density contrast in an overdensity, computed using linear theory, at the epoch when the collapsed object is deemed to have formed, is denoted by δ_c. We adopt the collapse of a spherical top-hat overdensity (Peebles 1980) as a valid model for the description of the dynamical evolution of the peaks in the Gaussian density distribution; the collapsed object is deemed to have 'formed' at the cosmic time t_c, which is approximately twice the cosmic time t_m at which the overdense region attains maximum expansion radius. In a universe with $\Omega_o = 1.0$, $\delta_c = 1.68$. It has been shown that δ_c varies by at most $\sim$4 per cent for a range of Ω_0 from 0.1 to 1 (Lacey & Cole 1993). Therefore, we have chosen to adopt a constant value 1.68 for δ_c.

In this Press–Schechter formalism, collapsed objects are identified on the basis of their overdensity assuming linear growth of perturbations. D_g, in equation (8), quantifies the growth factor of the density perturbations from the epoch of matter-radiation density equivalence ($z = z_{eq}$) to any later epoch z in the matter dominated era. In the absence of free streaming, the growth function is given by (Peebles 1980, Heath 1977)

$$D_g(z) = \frac{5\Omega_0}{2}(1+z_{eq})g(z)\int_z^\infty \frac{1+z'}{g(z')^3}\,\mathrm{d}z', \tag{9}$$

where

$$g^2(z) = \Omega_0(1+z)^3 + (1-\Omega_0-\Omega_\Lambda)(1+z)^2 + \Omega_\Lambda. \tag{10}$$

Closed-form expressions are available in Weinberg (1972), Groth & Peebles (1975) and Edwards & Heath (1976) for universes with and without a cosmological constant Λ; we have used these expressions for the purpose of our simulations.

The rms amplitude of the mass fluctuations at any redshift z: $\sigma(M,z)$, when smoothed with a spherically symmetric window function of characteristic comoving radius R, may be computed from the the matter power spectrum $P(k,z)$ using the relation:

$$\sigma^2(M,z) = \int_0^\infty \frac{\mathrm{d}k}{k}\frac{k^3}{2\pi^2}P(k,z)|\tilde{W}_R(k)|^2, \tag{11}$$

where $\tilde{W}_R(k)$ is the Fourier transform of the corresponding real space window function and, as before, $M = \frac{4}{3}\pi R^3\langle\rho\rangle$. A spherical top-hat form with radius R is usually adopted for the window function and this corresponds to a Fourier-space window function:

$$\tilde{W}_R(k) = \frac{3}{kR^3}[\sin(kR) - kR\cos(kR)]. \tag{12}$$

The Press–Schechter formalism has been verified by Tozzi & Governato (1998) against the results from numerical n-body dynamical simulations, particularly for the mass range encompassing clusters of galaxies.

4.2 P(k) and its normalization

We have adopted a power-law form for the initial primordial matter spectrum with $P_p(k) \sim k^n$, where n is the index of the primordial power spectrum; this index n equals unity for Harrison–Zel'dovich scale-invariant spectra. The power spectrum at any redshift z in the matter dominated era may then be written in the form

$$\frac{k^3}{2\pi^2}P(k,z) = \left(\frac{ck}{H_0}\right)^{3+n}\delta_H^2 T^2(k)D_g^2(z)/D_g^2(0), \tag{13}$$

where the D_gs are the growth factors defined in Section 4.1. δ_H represents the amplitude normalization of $P(k,z)$ and is defined as the amplitude of perturbations on the horizon scale at the present epoch $z = 0$.

The large-angle CMB anisotropies discovered by *COBE* (Smoot et al. 1992) are believed to have been generated by processes at the last scattering surface. They generated these anisotropies precisely for the reason that the matter fluctuations were of small fractional amplitudes at the epoch t, and because the scale length of the perturbation modes well exceeded ct, the coupling physics between the matter perturbations and radiation was linear and did not involve any astrophysical interactions. The CMB anisotropies detected by *COBE* may, therefore, be related to the primordial matter spectrum fairly exactly without all the uncertainties associated with the astrophysics involved in the formation of collapsed baryonic objects at late epochs. For this reason, we have chosen to normalize the $P(k)$ with the *COBE* results.

We have used the fitting formulae of Bunn & White (1997) to normalize the power spectrum to the *COBE-DMR* measurements. For an open universe with vanishing cosmological constant, with no CMB anisotropies coming from gravitational waves, we use the normalization

$$\delta_H = 1.95\times10^{-5}\Omega_0^{-0.35-0.19\ln\Omega_0-0.17\tilde{n}}\,\mathrm{e}^{-\tilde{n}-0.14\tilde{n}^2}, \tag{14}$$

$\tilde{n} = n - 1$ and the normalization is valid for $0.7 \leqslant n \leqslant 1.2$. The fit is also valid over the range 0.2–1.0 in Ω_0.

As mentioned earlier, the shape of $P(k,z)$ in the matter dominated era is completely determined by the transfer function $T(k)$ and the assumed form for the primordial spectrum. With the choice of a power-law form for $P_p(k)$, the transfer function is critical in relating the power on small wavenumber modes – which is fixed by the adopted *COBE* normalization – to those on large k modes at which we have clusters of galaxies. There are several fitting forms available in the literature for $T(k)$ in the context of the cold dark matter (CDM) dominated universes. However, different parametrizations of transfer functions can differ by large amounts (Peacock & Dodds 1993) and, moreover, to obtain better accuracy the effect of baryon damping must be included (Hu & Sugiyama 1996; Ma 1996; Eisenstein & Hu 1999). We, however, work within the context of low-baryon-density universes and, therefore, include the effect of non-zero baryon content by adopting a modified 'shape factor' Γ. In this work, we have adopted the fitting function provided by Bardeen et al. (1986):

$$T_{CDM}(q) = \frac{\ln(1+2.34q)}{2.34q}\times[1+3.89q+(16.1q)^2 + (5.46q)^3+(6.71q)^4]^{-1/4}, \tag{15}$$

where $q = k/h\Gamma$ and $\Gamma = \Omega_0 h\exp(-\Omega_B - \Omega_B/\Omega_0)$. Ω_B is the baryon density parameter and is the ratio of the mean density of baryons in the universe to the critical density $\rho_c = 3H_o^2/(8\pi G)$.

The Press–Schechter formalism described in Section 4.1, along with the *COBE*-normalized $P(k)$ defined above, have been used to calculate the number densities of collapsed objects. We choose to identify the condensates as groups/clusters of galaxies and have computed their abundances as a function of cluster mass and redshift for a set of CDM cosmologies differing in their Ω_o. We have not considered the effect of including a cosmological constant in this work and have put $\Lambda = 0$. The computations of cluster distributions $n(M,z)$ have been carried out over logarithmic

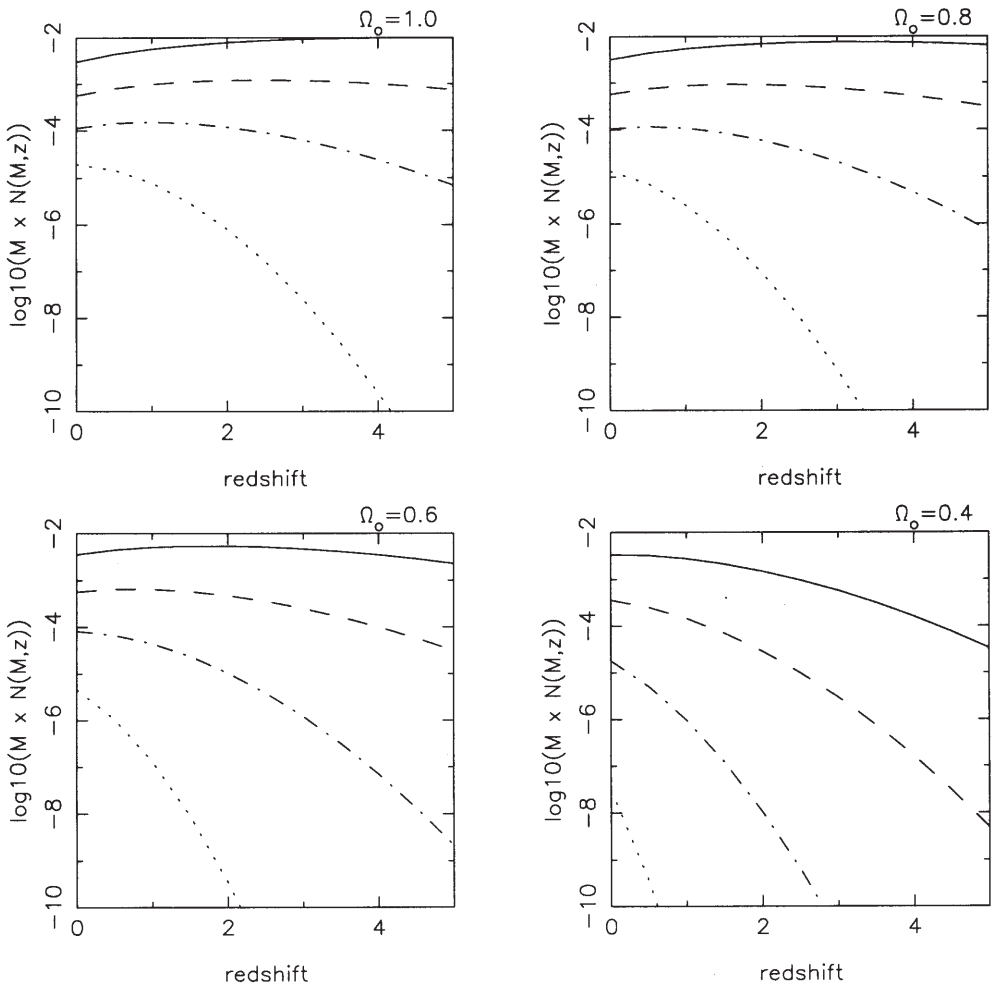

Figure 1. Abundance of objects with mass $M = 10^{12}\,\mathrm{M}_\odot$ (continuous line), $M = 10^{13}\,\mathrm{M}_\odot$ (dashed line), $M = 10^{14}\,\mathrm{M}_\odot$ (dot-dashed line) and $M = 10^{15}\,\mathrm{M}_\odot$ (dotted line). A CDM cosmology with $h = 0.65$, $\Lambda = 0$ and $\Omega_\mathrm{B} = 0.019\,h^{-2}$ is adopted; the four plots are labelled with the assumed values of Ω_o. The abundance $N(M, z)$ is expressed as the number of objects per Mpc^3 and $\log_{10}[M \times N(M, z)]$ is plotted versus redshift z.

bins in the mass range 10^{13}–$10^{16}\,\mathrm{M}_\odot$. The distribution in mass is computed at redshifts spaced at intervals of $\Delta z = 0.1$. Plots of $n(M, z)$ distributions are shown in Fig. 1.

The theory predicts that the cosmic abundance of massive collapsed objects are extremely sensitive to the amplitude and slope of the primordial power spectrum and also on the growth factor. In a flat cosmology with $\Omega_\mathrm{o} = 1$, $P(k)$ would grow as $(1 + z)^{-2}$; in an open universe the growth approximately follows this evolution down to redshift $z \approx (\Omega_\mathrm{o}^{-1} - 1)$ and is stunted thereafter. Therefore, in these models, which are all *COBE* normalized, the total growth up to the present time will be greater in models with larger Ω_o. Consistent with this reasoning, it may be seen in Fig. 1 that the larger Ω_o models are dynamically more evolved: they have larger numbers of $10^{15}\,\mathrm{M}_\odot$ objects at $z = 0$ and in these models the abundances of lower mass objects are declining with cosmic time as they are incorporated into larger mass objects.

It may be seen from Fig. 1 that the decline, with redshift, in the abundance of high-mass ($10^{15}\,\mathrm{M}_\odot$) collapsed objects relative to the abundance at $z = 0$ is steepest in the case of models with lower Ω_o. This is the opposite of the expectations for models which are normalized at the present time to, for example, a specific value of σ_8, which is the rms mass fluctuations when the present day universe is smoothed using a window function with a radius $R = 8\,h^{-1}\,\mathrm{Mpc}$. Although the growth function evolves slower at low redshifts in models with low Ω_o, the abundance of massive collapsed objects evolves more strongly in the case of the low Ω_o models because in these models the rms mass fluctuations $\sigma(M, z)$ is itself low at $z = 0$.

The Gaussian characteristic of the Press-Schechter mass function is evident in the distributions: at any redshift, there is a rapid exponential decline in the number density of objects in larger mass bins.

4.3 Simulated sky images

Our simulation codes compute the abundances $n(M, z)$ in redshift slices in the redshift range $z = 0$–5. We make the conservative assumption that collapsed objects in the restricted range 10^{13}–$10^{16}\,\mathrm{M}_\odot$ alone represent clusters of galaxies containing hot gas. Adopting a model, described below, for the spatial distribution of hot gas in the potential wells of these clusters, we simulate sky images of the S–Z effect expected owing to these clusters. The sky was simulated by separately computing the contributions from different redshift slices along the line of sight. In any redshift slice, the clusters are assumed to be Poisson-random distributed

on the sky. We have simulated square patches of sky consisting of 256 pixels along each side: the pixels were chosen to be 10 arcsec square making the total image size $42'40''$. The redshift slices were of size $\Delta z = 0.1$.

The mean number of clusters, λ, with mass in the range $M - (M + \delta M)$, is related to the Press-Schechter number density by:

$$\lambda = n(M, z) \times \delta M \times \text{volume corresponding to a pixel.} \quad (16)$$

The comoving volume of any pixel in a slice at redshift z is calculated as the product of the comoving area $(\Delta l)^2$ covered by the square pixels of angular size $\Delta\theta = 10$ arcsec and the comoving line-of-sight distance Δs corresponding to the redshift slice Δz. These are given by:

$$\Delta s = \frac{c}{H_0} \frac{\mathrm{d}z}{(1+z)\sqrt{1+\Omega_{\mathrm{o}} z}}, \quad (17)$$

and

$$\Delta l = \frac{2c\Delta\theta}{H_{\mathrm{o}}\Omega_{\mathrm{o}}^2(1+z)} \{\Omega_{\mathrm{o}} z + (\Omega_{\mathrm{o}} - 2)[\sqrt{\Omega_{\mathrm{o}} + 1} - 1]\}. \quad (18)$$

We have associated every collapsed massive object, with mass exceeding $10^{13}\,\mathrm{M}_\odot$, with cluster gas. In order to model the spatial distribution of the intracluster gas, the isothermal β model has been adopted, in which the cluster gas is modelled as being spherically symmetrical, centred in the gravitational potential of the cluster and shock heated to a temperature corresponding to the infall energy. The variation in gas density with radial distance r is assumed to be given by

$$\rho(r) = \rho_0[1 + (r/r_{\mathrm{c}})^2]^{-3\beta/2}, \quad (19)$$

where ρ_{o} is the central density and r_{c} is the core radius. The value of β, inferred from the X-ray surface-brightness profiles observed in clusters of galaxies, is believed to be in the range 0.5–0.9 (Markevitch et al. 1998, Jones & Forman 1984). Herein, for simplicity, we adopt a value of 2/3 for β.

Assuming that the dynamical collapse of the cluster is self similar, the scaling of the core radius r_{c} of collapsed objects with mass and redshift has been derived to have the form (Kaiser 1986; Colafrancesco 1997):

$$r_{\mathrm{c}}(\Omega_0, M, z) = \frac{1.3\,h^{-1}\,\mathrm{Mpc}}{p} \frac{1}{(1+z)} \times \left[\frac{M}{10^{15}\,h^{-1}\,\mathrm{M}_\odot} \frac{\Delta(\Omega_0 = 1, z = 0)}{\Omega_0 \Delta(\Omega_0, z)}\right]^{1/3}. \quad (20)$$

In this parametrization, the non-linear density contrast at the epoch of virialization is $\Delta = \tilde{\rho}/\rho$, where $\tilde{\rho}$ is the density contrast and ρ is the mean background density. For the case of an open universe,

$$\Delta = \frac{18\pi^2}{\Omega_0 H_0^2 t_{\mathrm{v}}^2} \frac{1}{(1+z_{\mathrm{v}})^3}, \quad (21)$$

where t_{v} and z_{v} are the cosmic time and redshift corresponding to the epoch of virialization. In the case of a flat universe, $\Delta \approx 178$ (Peebles 1980; Colafransesco et al. 1997). In the above parametrization, p is an adjustable free parameter that may be selected to fit observations of nearby clusters. If r_{m} denotes the maximum radial extent of the cluster, $p = (r_{\mathrm{m}}/r_{\mathrm{c}})$ and is a measure of the concentration of the cluster mass: small values of p model the cluster gas as centrally concentrated whereas larger values of p spread the gas mass away from the core. Values of $p \approx 6$ appear to better model the parameters of nearby clusters; a comparison of the model with the observed parameters for the Coma cluster is given below. We propose to use the simulations for the purpose of predicting the sky variance as observed by the Australia Telescope Compact Array (ATCA); these observations are made with arcmin resolution and will be less sensitive to S–Z effects from clusters whose gas distribution is extended. The ATCA observations couple somewhat better to models with smaller p; therefore, we have adopted the conservative choice of $p = 8$. It may be noted that sensitive X-ray imaging of the gas in nearby clusters have shown gas extending out to at least eight core radii.

Although recent observations indicate that intracluster gas has temperature structure (Markevitch et al. 1998), we have modelled the clusters as being isothermal. It follows from the assumption that clusters form from self-similar collapse that the temperature $T \propto (M/R)$ and a good approximation for the temperature of the intracluster gas in clusters is (Colafrancesco et al. 1997)

$$T = 6.7 \times 10^7 (1+z) \left[\frac{M}{10^{15}\,h^{-1}\,\mathrm{M}_\odot}\right]^{2/3} \left[\frac{\Omega_0 \Delta(\Omega_0, z)}{\Delta(\Omega_0 = 1, z = 0)}\right]^{1/3} \mathrm{K}. \quad (22)$$

The relation between the mass and the temperature in equation (22) agrees well with the recent $M - T$ parametrization as suggested by Bryan & Norman (1998). We have assumed that the hot gas detected in its X-ray emission is responsible for any S–Z effect as well (Colafrancesco et al. 1994; Blanchard et al. 1992; Vittorio et al. 1997; Kaiser 1986).

Only the baryonic matter in collapsed clusters gives the S–Z effect. White et al. (1993) have estimated the baryon content in clusters to be

$$\frac{M_{\mathrm{b}}}{M_{\mathrm{tot}}} \geqslant 0.009 + 0.050\,h^{-3/2}, \quad (23)$$

where the first contribution is due to the galaxies and the second is due to the intracluster gas. Primordial nucleosynthesis predicts a universal baryon abundance $\Omega_b \simeq 0.019\,h^{-2}$ (Burles, Nottel & Turner 1999). Adopting the Hubble parameter $h = 0.65$, it is seen that the baryon gas-mass fraction in nearby clusters is about 0.1 and is a factor of two greater than the universal baryon abundance. The *Einstein* Medium Sensitivity Survey (EMSS) data appears to indicate a decline in the abundance of X-ray luminous clusters with redshift (Henry et al. 1992); this may be parametrized as a hot-gas fraction that evolves as $t^{1.4}$ with cosmic epoch. It may be noted that adopting a gas fraction that declines with redshift is a conservative assumption because it reduces the predicted S–Z effect. We have adopted a parametrization

$$\frac{M_{\mathrm{gas}}}{M_{\mathrm{tot}}} = 0.050\,h^{-3/2} \left[\frac{M_{\mathrm{tot}}}{10^{15}\,h^{-1}\,\mathrm{M}_\odot}\right]^{0.2} \left[\frac{t}{t_{\mathrm{o}}}\right]^q, \quad (24)$$

with $q = 1.4$. M_{gas} represents the hot gas mass in the cluster and M_{tot} represents the total mass in the collapsed object. The exponent 0.2 in equation (24) is from a fit in Colafrancesco et al. (1997). We have assumed that the intracluster gas has a primordial composition, with helium and hydrogen atoms in the number ratio 1:10, and is fully ionized.

The cluster mass distribution, as also the intracluster gas, are modelled as truncated at a maximum radius $r_m = p \times r_c$. We define the 'impact parameter' b as the projected distance between the cluster centre and any line of sight through the cluster. It

follows that the S–Z decrement in the Rayleigh-Jeans portion of the spectrum, in units of temperature, expected at any sky position $b \lesssim r_{\max}$ is given by

$$\Delta T = -T_{\rm CMB}\frac{2kT}{m_{\rm e}c^2}\times\int_b n_{\rm e}\sigma_T\,{\rm d}l, \tag{25}$$

where $T_{\rm CMB}$ is the average brightness temperature of the CMB. The integral is computed along the line of sight through the cluster at the impact parameter b.

The assumption that the cluster gas is of primordial composition implies that the total number of hot electrons in the cluster is $N_{\rm e} = (18/14)(M_{\rm gas}/{\rm a.m.u})$. The S–Z decrement may be written in the form

$$\Delta T/T_{\rm CMB} = -\frac{2kT}{m_{\rm e}c^2}\sigma_{\rm T} \times\frac{1}{4\pi}\frac{\tan^{-1}\left(\sqrt{r_{\max}^2-b^2}/\sqrt{r_c^2+b^2}\right)N_{\rm e}r_c}{\sqrt{r_c^2+b^2}[r_c r_{\max}-r_c^2\tan^{-1}(r_{\max}/r_c)]}. \tag{26}$$

The Coma cluster at a redshift 0.0235, with a total mass about $2\times10^{15}\,{\rm M}_\odot$, is observed to have X-ray gas with a temperature 8–9 keV and a core radial size of 10.5 arcmin (Silverberg et al. 1997, Herbig et al. 1995). The Compton-y parameter has been measured to be 9×10^{-5} towards its centre (Herbig et al. 1995). In our simulations, for the choice $p = 6$ and adopting a value of 0.096 as the baryon gas fraction, we find that a collapsed object of mass $2\times10^{15}\,{\rm M}_\odot$ at redshift $z = 0.0235$ – corresponding to the Coma cluster parameters – yields values of 10.3–11.0 arcmin for the core size, 8–9×10^7 K for the gas temperature and the central S–Z Compton-y decrement is in the range 7–8.5×10^{-5}.

We have accumulated the S–Z effect from clusters in redshift slices up to a maximum redshift of 5. In each redshift slice, the pixels were populated by collapsed point masses in a Poisson random fashion; the expectation that any pixel was populated by objects in any mass bin was governed by equation (16). We then substituted our cluster gas model for every mass point: the S–Z effect owing to each cluster is distributed over several pixels surrounding that at which the point mass was located. The variance of the temperature fluctuations in the cumulative S–Z effect images were computed.

We have compared the results of the simulations with the observational limits on arcmin-scale CMB anisotropy set by the ATCA experiment at 8.7 GHz (Subrahmanyan et al. 1993, 1998,

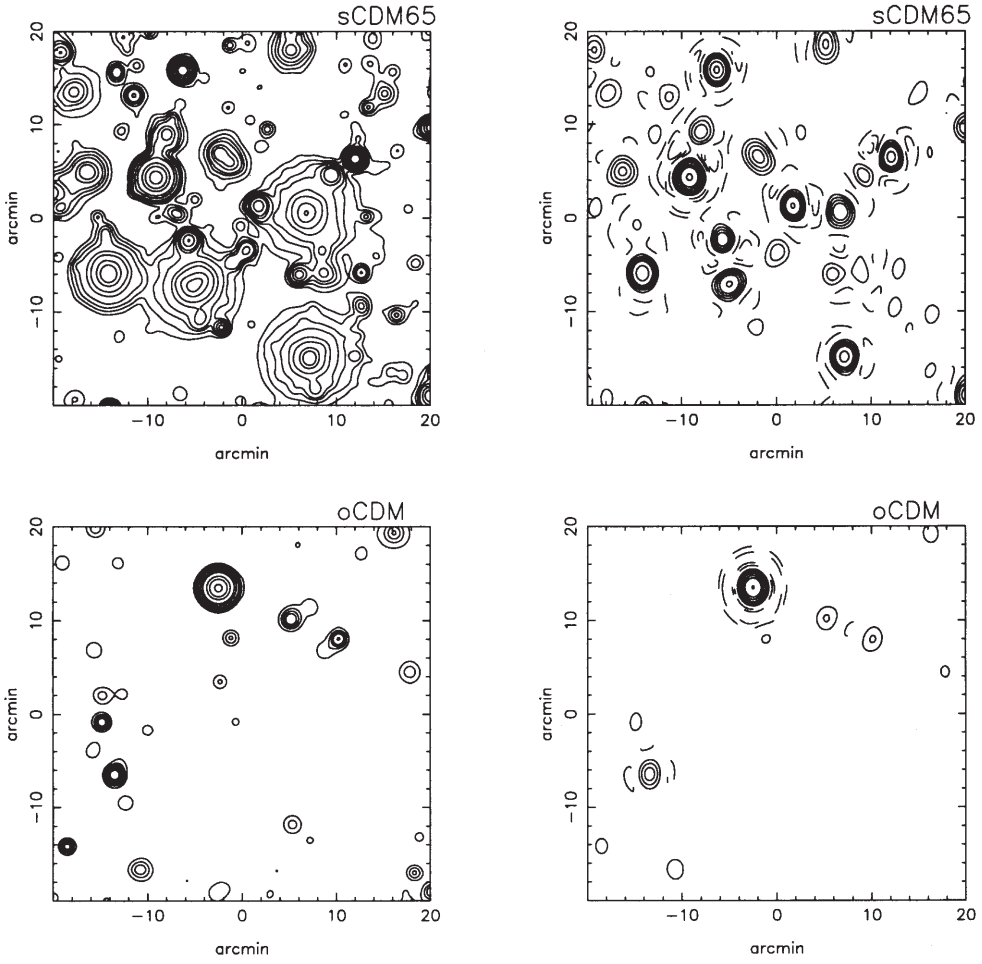

Figure 2. Sample images. The upper pair of images corresponds to CDM cosmology with $\Omega_\circ = 1.0$; the lower pair corresponds to $\Omega_\circ = 0.6$. The cluster gas distribution has been parametrized with $p = 8$ and the baryon gas fraction is assumed to evolve with redshift as described by equation (24); the Hubble parameter $h = 0.65$ has been adopted. The images on the left have been convolved with a Gaussian beam of FWHM 1 arcmin; the images on the right have been convolved by the ATCA product beam. Contours at $(-3, -2, -1, 1, 2, 3, 4, 6, 8, 12, 16, 24)\times-30\,\mu$K for the images on the left and $-30\,\mu$Jy beam^{-1} for the images on the right.

1999). These observations have been made with a Fourier synthesis array. The sky is viewed by the telescope as attenuated by a primary beam that has a full width at half maximum of about 6 arcmin and the synthetic images represent the convolution of the visible sky with a synthetic beam pattern. The ATCA experiment sets upper limits on any residual sky fluctuations apart from the instrument noise and confusing foreground sources. Assuming 'flat-band' CMB fluctuations, the ATCA limit corresponds to $Q_{\rm flat} \lesssim 25\,\mu$K and, for their telescope filter function, this corresponds to an upper limit of $21\,\mu$Jy beam^{-1} on the flux-density fluctuations on the sky. We have convolved the images resulting from our simulations by a beam that is the product of the ATCA synthetic beam and primary beam. Sample images are shown in Fig. 2 corresponding to CDM models with $\Omega_{\rm o} = 1.0$ and 0.6. Images are displayed using a 1-arcmin Gaussian (normalized to give unity volume) as the convolving beam and separately using the ATCA product beam (normalized to have a peak unity) as the convolving function. It is seen that the extended clusters, seen in the $\Omega_{\rm o} = 1.0$ simulation, are resolved by the ATCA beam: the extended S–Z structures will not be detectable by the ATCA imaging. It may be noted that before the convolution, the image pixels are in units of temperature (K); following the convolution, the pixel intensities are in units of flux density (Jy beam^{-1}). The predictions for the image variance have been made for different plausible cosmological models.

5 RESULTS AND DISCUSSION

Results of the simulations are given in Table 1 for a range of model parameters. The image variances have been listed both before and after convolving with the ATCA product beam. The standard CDM model with $h = 0.5$, $\Omega_{\rm o} = 1.0$ and with the hot gas fraction parametrized as described in equation (24), is expected to result in an image rms which exceeds the ATCA limit. Increasing the Hubble parameter to a more likely value of $h = 0.65$ increases the expectations for the image rms and this 'high-h' CDM model is rejected with greater confidence. Considering open universe CDM models with $\Omega_{\rm o} < 1$, the expected image variance decreases with decreasing $\Omega_{\rm o}$. Low $\Omega_{\rm o} < 0.8$ open-universe models are allowed by the ATCA limits.

If we assume that $q = 0$ and that the cluster gas fraction does not diminish with redshift, high-redshift clusters contribute to the net S–Z sky fluctuations. This is seen in the table where the image rms rises from 28 to $72\,\mu$Jy beam^{-1} when the no-evolution assumption is made for the standard CDM model. We have also simulated images corresponding to the case where the gas fraction is a constant and equal to the mean baryon density predicted by nucleosynthesis. This gas model leads to predicted rms values which are not very different from that given by the $q = 0$ parametrized model; this indicates that the lower mass ($M_{\rm tot} \approx 10^{13\text{–}14}\,{\rm M}_{\odot}$) objects dominate the variance contribution in the no-evolution case.

Simulations of images corresponding to the choice $p = 6$ leads to enhancements in the expectations of the image rms values confirming that our earlier choice ($p = 8$) was relatively conservative.

We have computed the mean Compton-y parameter from the images for the different models and these are also listed in Table 1. The *COBE*-FIRAS (Far Infrared Absolute spectrometer) experiment has set an upper limit of $y < 1.5 \times 10^{-5}$ (Fixsen et al. 1996). It may be noted that our CDM model with $h = 0.65$ is independently rejected by these limits. Likewise, the models with no evolution in gas fraction are also disallowed by the FIRAS results.

The value of σ_8 has also been computed for each model and listed in Table 1. The standard CDM models normalized to *COBE* are known to be incompatible with estimates of σ_8 derived from the local X-ray luminosity function or other local measures of galaxy clustering (which prefer low values of σ_8 about 0.6). The ATCA results independently provide evidence in favour of a low-$\Omega_{\rm o}$ universe. It must be emphasized once again that the sky fluctuations due to SZE is generically non-Gaussian in nature and a precise elimination of models have to take this into account.

An important difference between this work as compared to previous predictions for CMB anisotropies from S–Z effects is that we have normalized our matter power spectrum to the *COBE* anisotropy results. All the previous predictions that we are aware of have normalized their models to observations of the present day clustering in galaxies or to X-ray luminosity functions; consequently, other workers have essentially normalized their matter power spectra to σ_8. This makes it possible for all the models to be consistent with the observational estimates of present day cluster abundances. Our choice of *COBE* normalization results in a σ_8 that varies across the models. This results in a dependance on $\Omega_{\rm o}$ which is opposite of what is usually found. The difference may be understood in the following way: if the σ_8 is held constant across cosmological models, as previous workers have done, varying $\Omega_{\rm o}$ changes the growth function and consequently the abundance of clusters at redshifts $z > 0$ will decrease with increasing $\Omega_{\rm o}$. On the other hand, when the matter power spectrum is normalized to *COBE-DMR* data, varying $\Omega_{\rm o}$ across models alters the shape of the matter spectrum and the normalization in addition to the growth function. In this case, increasing

Table 1. Statistics for different cosmological models.

Model	Ω_0	h	σ_8	gas fraction[a]	mean y $\times 10^{-5}$	Image rms before convolution (μK)	Image rms after convolution (μJy beam^{-1})
sCDM	1.0	0.50	1.128	parametrized	0.61	81	28
sCDM(high h)	1.0	0.65	1.567	parametrized	1.9	313	58
oCDM1	0.8	0.65	1.326	parametrized	0.46	60	23
oCDM2	0.6	0.65	1.004	parametrized	0.18	38	15
oCDM3	0.4	0.65	0.605	parametrized	0.05	9	3
sCDM(variant1)	1.0	0.50	1.128	no evolution	1.9	207	72
sCDM(variant2)	1.0	0.50	1.128	$\frac{M_{\rm gas}}{M_{\rm tot}} = \Omega_B$	2.4	245	79
sCDM(p = 6)	1.0	0.50	1.128	parametrized	1.16	98	37

[a] The parametrization of the gas fraction is described in equation (24).

Ω_o results in an increase in cluster abundances at all redshifts. Our choice of normalization results in a σ_8 that varies across the models.

6 CONCLUSION

We have considered cosmological models composed of cold dark matter and baryons (and no cosmological constant), having an initial scale-invariant spectrum of adiabatic perturbations. We have used the Press–Schechter formalism to generate the distribution of clusters. We have normalized the rms mass fluctuations to *COBE-DMR* data. The Sunyaev–Zel'dovich decrement is calculated for each cluster adopting a model for the density profile of the cluster gas. We have simulated blank sky surveys for the S–Z effect owing to a cosmological distribution of clusters. Finally, we have predicted the expectations for the variance in the background sky both before and after convolving with the ATCA beam. Based on a comparison with the upper limits set by the ATCA on CMB anisotropies on arcmin scales, we conclude that *COBE*-normalized CDM models of the universe with a high density parameter ($\Omega_o > 0.8$) are rejected. This result is independent of any present epoch measures of σ_8.

ACKNOWLEDGMENTS

SM would like to thank Dr. Pijushpani Bhattacharjee for his constant encouragement, Dr Biman Nath for many valuable discussions and Dipanjan Mitra for helping with the computers. SM also wishes to thank 'everyone@rri' for their hospitality and warmth and for providing access to the computer facility.

REFERENCES

Aghanim N., Desert F. X., Puget J. L., Gispert R., 1996, A&A, 311, 1
Barbosa D., Bartlett J. G., Blanchard A., Oukbir J., 1997, in Bouchet F., Gispert R., Guiderdoni B., Jean Tran Thanh Van, eds, Microwave Background Anisotropies, Proceedings of XIV Moriond Astrophysics Meetings
Bartlett J. G., 1997, in Valls-Gabaud D., Hendry M. A., Molaro P., Chamcham K., eds, ASP Conf. Ser. Vol. 126, From Quantum Fluctuations to Cosmological Structures. Astron. Soc. Pac., San Francisco, p. 365
Bartlett J. G., Silk J., 1994, ApJ, 423, 12
Birkinshaw M., 1999, Phys. Rep., 310, 97
Blanchard A., Bartlett J. G., 1998, A&A, 332, 49L
Blanchard A., Valls-Gabaud D., Mamon D. A., 1992, A&A, 264, 365
Bond J. R., Crittenden R., Davis R. L., Efstathiou G., Steinhardt P. J., 1994, Phys. Rev. Lett., 72, 13
Bryan G. L., Norman J. L., 1998, ApJ, 495, 80
Bunn E. F., White D., 1997, ApJ, 480, 6
Burles S., Nottel K. M., Turner M. S., astro-ph/9903300
Colafrancesco S., Mazzotta P., Rephaeli Y., Vittorio N., 1994, ApJ, 433, 454
Colafrancesco S., Mazzotta P., Rephaeli Y., Vittorio N., 1997, ApJ, 479, 1
Edwards D., Heath D., 1976, Ap&SS, 41, 183
Eisenstein E. J., Hu W., 1999, ApJ, 511, 5
Evrard A. E., 1990, in Oegerle W. R., Fitchett M. J., Danly L., eds, Clusters of Galaxies, Cambridge University Press, New York
Evrard A. E., Metzler C. A., Navarro J. F., 1996, ApJ, 469, 494
Fixsen D. J., Cheng E. S., Gales J. M., Mather J. C., Shafer R. A., Wright E. L., 1996, ApJ, 473, 576
Groth E. J., Peeble P. J. E., 1975, A&A, 41, 143
Heath D. J., 1977, MNRAS, 179, 351
Henry J. P., Gioia I. M., Maccacaro T., Morris S. L., Stocke J. T., Wolter A., 1992, ApJ, 386, 408
Herbig T., Lawrence C. R., Redhead A. C. S., Gulkis S., 1995, ApJ, 449, L5
Hu W., Sugiyama N., 1996, ApJ, 471, 54
Hu W., Scott D., Silk J., 1994, Phys. Rev. D., 49, 2
Jones C., Forman W., 1984, ApJ, 276, 38
Jones M. et al., 1997, ApJ, 479, L1
Kaiser N., 1986, MNRAS, 222, 323
Kamionkowski M., Spergel D. L., 1994, ApJ, 432, 7
Lacey C., Cole S., 1993, MNRAS, 262, 627
Lineweaver C. H., Barbosa D., 1998, ApJ, 496, 624
Ma C. P., 1996, ApJ, 471, 13
Markevitch M., Forman W. R., Sarazin C. L., Vikhlinin A., 1998, ApJ, 504, 27
Oukbir J., Blanchard A., 1992, A&A, 262, L21
Oukbir J., Blanchard A., 1997, A&A, 317, 1
Padmanabhan T., 1993, Structure Formation in the Universe. Cambridge University Press, Cambridge
Padmanabhan T., Subramanian K., 1992, Bull. Astron Soc. India, 20, 1
Peacock J. A., Dodds S. J., 1994, MNRAS, 267, 1020
Peebles P. J. E., 1980, Large Scale Structure of the Universe. Princeton University Press, Princeton
Perlmutter S. et al., 1998, Nat, 391, 51
Persi F. M., Spergel D. N., Cen R., Ostriker J. P., 1995, ApJ, 442, 1
Press W. H., Schecter P., 1974, ApJ, 187, 225
Richards E. A., Fomalont E. B., Kellermann K. I., Partridge R. B., Windhorst R. A., 1997, AJ, 113, 1475
Silverberg R. F. et al., 1997, ApJ, 485, 22
Smoot G. F. et al., 1992, ApJ, 396, L1
Subrahmanyan R., Ekers R. D., Sinclair M., Silk J., 1993, MNRAS, 263, 416
Subrahmanyan R., Kesteven M. J., Ekers R. D., Sinclair M., Silk J., 1998, MNRAS, 298, 1189
Subrahmanyan R., Kesteven M. J., Ekers R. D., Sinclair M., Silk J., 1999, MNRAS, submitted
Sunyaev R. A., Zel′dovich Ya. B., 1972, Comm. Astrophys. Space Phys., 4, 173
Tozzi P., Governato F., 1998, in Fontana A., Giallongo E., eds, ASP Conf. Ser. Vol. 146, The Young Universe: Galaxy formation at Intermediate and High Redshifts. Astron. Soc. Pac., San Francisco, p. 461
Vittorio N., Colafranseco S., Mazzotta P., Rephaeli Y., 1997, in Bouchet F., Gispert R., Guiderdoni B., Jean Tran Thanh Van, eds, Microwave Background Anisotropies, Proceedings of XIV Moriond Astrophysics Meetings
Weinberg S., 1972, Gravitation and Cosmology. Wiley, New York
White S. D. M., Navarro J. F., Evrard A. E., Frenk C. S., 1993, Nat, 366, 429

This paper has been typeset from a TEX/LATEX file prepared by the author.